Research article

Olga V. Borovkova*, Felix Spitzer, Vladimir I. Belotelov, Ilya A. Akimov*, Alexander N. Poddubny, Grzegorz Karczewski, Maciej Wiater, Tomasz Wojtowicz, Anatoly K. Zvezdin, Dmitri R. Yakovlev and Manfred Bayer

Transverse magneto-optical Kerr effect at narrow optical resonances

https://doi.org/10.1515/nanoph-2018-0187
Received November 2, 2018; revised December 4, 2018; accepted December 6, 2018

Abstract: Magneto-optical spectroscopy based on the transverse magneto-optical Kerr effect (TMOKE) is a sensitive method for investigating magnetically-ordered media. Previous studies were limited to the weak coupling regime where the spectral width of optical transitions considerably exceeded the Zeeman splitting in magnetic field. Here, we investigate experimentally and theoretically the transverse Kerr effect in the vicinity of comparatively narrow optical resonances in confined quantum systems. For experimental demonstration we studied the ground-state exciton resonance in a (Cd,Mn)Te diluted magnetic semiconductor quantum well, for which the strong exchange interaction with magnetic ions leads to giant Zeeman splitting of exciton spin states. For low magnetic fields in the weak coupling regime, the Kerr effect magnitude grows linearly with increasing Zeeman splitting showing a dispersive S-shaped spectrum, which remains almost unchanged in this range. For large magnetic fields in the strong coupling regime, the magnitude saturates, whereas the spectrum becomes strongly modified by the appearance of two separate peaks. TMOKE is sensitive not only to the sample surface but can also be used to probe in detail the confined electronic states in buried nanostructures if their capping layer is sufficiently transparent.

Keywords: Nanophotonics; semiconductor nanostructures; excitons; magneto-optics; magneto-optical Kerr effects.

***Corresponding authors: Olga V. Borovkova,** Russian Quantum Center, 143025 Skolkovo, Moscow Region, Russia, e-mail: o.borovkova@rqc.ru. https://orcid.org/0000-0002-0577-7658; and **Ilya A. Akimov,** Experimentelle Physik 2, Technische Universität Dortmund, 44221 Dortmund, Germany; and Ioffe Institute, Russian Academy of Sciences, 194021 St. Petersburg, Russia, e-mail: ilja.akimov@tu-dortmund.de
Felix Spitzer: Experimentelle Physik 2, Technische Universität Dortmund, 44221 Dortmund, Germany
Vladimir I. Belotelov: Russian Quantum Center, 143025 Skolkovo, Moscow Region, Russia; and Moscow State University, 119991 Moscow, Russia
Alexander N. Poddubny: Ioffe Institute, Russian Academy of Sciences, 194021 St. Petersburg, Russia
Grzegorz Karczewski and Maciej Wiater: Institute of Physics, Polish Academy of Sciences, 02668 Warsaw, Poland
Tomasz Wojtowicz: International Research Centre MagTop, Institute of Physics, Polish Academy of Sciences, 02668 Warsaw, Poland
Anatoly K. Zvezdin: Russian Quantum Center, 143025 Skolkovo, Moscow Region, Russia; and Prokhorov General Physics Institute RAS, Moscow 119991, Russia
Dmitri R. Yakovlev and Manfred Bayer: Experimentelle Physik 2, Technische Universität Dortmund, 44221 Dortmund, Germany; and Ioffe Institute, Russian Academy of Sciences, 194021 St. Petersburg, Russia

1 Introduction

The transverse magneto-optical Kerr effect (TMOKE) is one of the magneto-optical effects that emerge due to the Zeeman splitting of the electron levels in magnetic field [1]. Contrary to the widely used Faraday effect, TMOKE is sensitive to the spin component orthogonal to the light propagation direction and is usually used to detect the in-plane magnetization of para- and ferromagnetic materials [2–5].

Furthermore, TMOKE is an intensity effect of an incident light beam that is defined by the relative change of reflectance R for the two opposite directions of an in-plane magnetic field $\mathbf{B}$:

$$\delta = 2\frac{R(\mathbf{B}) - R(-\mathbf{B})}{R(\mathbf{B}) + R(-\mathbf{B})}. \quad (1)$$

TMOKE appears only for oblique light incidence with the magnetic field orthogonal to the incidence plane and in a frequency range where the medium's absorption is nonvanishing [1]. As TMOKE is related to the modification of boundary conditions for the incident light by the magnetic field, it is valuable for the investigation of magnetic properties near the sample's interface [2, 3]. If the boundary conditions at two interfaces of a thin magnetic film are different, the transmitted light intensity becomes magnetization dependent as well [6].

Usually, TMOKE is observed for ferromagnetic metals in the visible and infrared spectral range, where it has a typical value of $\delta \approx 10^{-3}$ and a weak spectral dependence [7]. In dielectric materials, the off-resonant TMOKE in the transparency range is very weak due to the negligible absorption. However, resonant TMOKE with notable magnitude may be present even in nearly transparent media in the vicinity of the absorption band, which is provided by spectrally narrow optical resonances. Such phenomenon has been recently actively studied in hybrid magnetophotonic structures where the optical resonances are represented by electromagnetic modes such as surface plasmon polaritons [8, 9], waveguide modes [10, 11], or optical Tamm states [12]. It was demonstrated that TMOKE is drastically enhanced in hybrid metal-dielectric structures at the resonance of surface plasmon-polaritons [8, 13–16] and reaches up to $\delta = 0.15$ (see Ref. [17]). Nevertheless, due to the strong absorption in metals, the bandwidth of the plasmonic resonances Γ significantly exceeds the Zeeman splitting Δ, so that the ratio $\Delta/\Gamma \ll 1$ holds. In this case, the spectral dependence of TMOKE has a characteristic S-shape around the plasmonic resonance: it possesses maxima and minima at the slopes of the resonance and crosses zero at the central frequency.

Further types of optical resonances are represented, for instance, by confined quantum states such as rare earth ions in dielectrics [18, 19] or excitons in semiconductors [20]. Recently, the enhancement of the polarization magneto-optical effects near the excitonic resonance has been addressed [21].

Optical resonances related to confined quantum states are much narrower as compared to plasmonic excitations. Therefore, the fundamentally new strong coupling regime with $\Delta/\Gamma \geq 1$ can be established, where the exciton damping Γ is slower compared to its spin precession in a magnetic field. Consequently, the Zeeman splitting is observed in reflectivity in contrast to the weak coupling regime with $\Delta/\Gamma \leq 1$. Surprisingly, TMOKE was not yet studied in this regime irrespective of the studied system.

In this work, we reveal TMOKE in the vicinity of narrow optical resonances that originate from excitons. For demonstration purposes, we focus on excitons in diluted magnetic semiconductor (DMS) quantum well (QW) structures. Here, the exchange interaction of magnetic ions with the conduction band electrons ($s - d$) and valence band holes ($p - d$) allows to achieve a large exciton Zeeman splitting with $\Delta/\Gamma > 1$ already in moderate magnetic fields [20, 22, 23]. In particular, we demonstrate the enhancement of TMOKE in the vicinity of exciton resonances in a 10-nm-thick (Cd,Mn)Te/(Cd,Mg)Te QW. We should underline that although TMOKE is used to be sensitive to the surface effects, in case of relatively transparent cap layer as it happens in the addressed semiconductor QW structures, TMOKE serves as an efficient probe tool for the confined states in depth, where the QW is located.

In what follows, first, we consider TMOKE theoretically for a generic three-level system and confirm that the TMOKE features observed at the exciton resonance are inherent to a broad class of optical resonances caused by confined quantum states. Second, we demonstrate resonant TMOKE for spectrally narrow excitonic resonances in a (Cd,Mn)Te/(Cd,Mg)Te QW structure.

2 Results

2.1 Theory of TMOKE near the resonance of a three-level system

In order to identify the general properties of TMOKE in the vicinity of a spectrally narrow optical resonance, let us theoretically study TMOKE in a simplified magneto-optical model for the electric dipole optical transitions in a three-level quantum system, which is realized in a large variety of atomic, molecular, and solid-state objects with pseudospin in the excited or ground state [24–26]. In particular, one example of such systems is represented by a single level in the ground state (g), which is coupled through the optical field to two excited states (e, with pseudospin projection $S_y = \pm\frac{1}{2}$). The latter are split due to the Zeeman effect. The selection rules for optical transitions dictate that excitation with an electromagnetic wave, which possesses σ^+ circular polarization in the xz-plane, addresses the state with angular momentum projection $S_y = +\frac{1}{2}$ and correspondingly $S_y = -\frac{1}{2}$ for σ^- polarization. Due to the Zeeman splitting Δ, their energies are split from the central one E_0 by $\Delta/2$: $E = E_0 \pm \Delta/2$ (see Figure 1A).

These transitions cause resonances in the permittivity tensor $\varepsilon_{ij} = \varepsilon\delta_{ij} - \mathrm{i}e_{ijk}g_k$, where g_k is the gyration vector, e_{ijk} is the Levi-Civita tensor, and $i, j, k = x, y, z$ [1]. In the case of the magnetic field directed along the y-axis, the permittivity tensor components are

$$\varepsilon = \varepsilon_\mathrm{b}\left(1 + \frac{4\pi|\mathbf{d}|^2}{\varepsilon_\mathrm{b}}\frac{E_0 - E - \mathrm{i}\Gamma}{(E_0 - E - \mathrm{i}\Gamma)^2 - (\Delta/2)^2}\right),$$
$$g_y = \frac{2\pi|\mathbf{d}|^2\,\Delta}{(E_0 - E - \mathrm{i}\Gamma)^2 - (\Delta/2)^2};\ g_x = 0;\ g_z = 0, \tag{2}$$

where E is the energy, ε_b is the background permittivity, $\mathbf{d}$ is the matrix element of the electron transition dipole moment, and Γ is the damping.

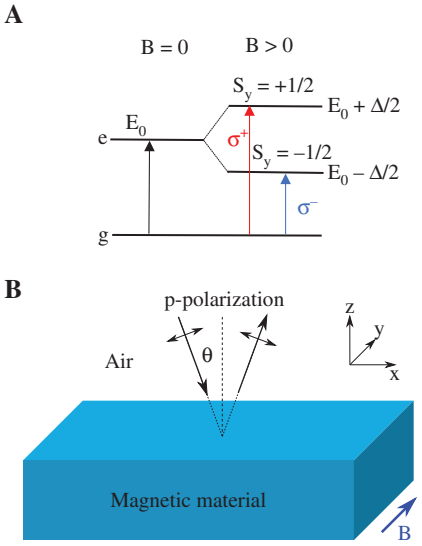

Figure 1: (A) Scheme of the optical transitions in a three-level system composed of the ground level (g) and two excited states (e), which are split off due to the Zeeman effect in magnetic field B||*y*. (B) Geometry of the considered setting, where *p*-polarized light is reflected from a semi-infinite magnetic medium with a three-level resonance shown in (A).

Relatively simple analytical expressions for TMOKE [Supplementary Eq. (S1)] can be obtained for the light reflection from a semi-infinite magnetic medium. The principle scheme of the considered geometry of the light incidence and the applied magnetic field is shown in Figure 1B.

We start the asymptotic analysis of Eq. (S1) for the weak coupling regime ($\Delta/\Gamma \ll 1$), which gives the following expression for TMOKE [see Supplementary Eq. (S2)]:

$$\delta = -\frac{8E_d \Delta\Gamma \tan\theta}{\varepsilon_b - 1} \frac{\tilde{E}}{[(\tilde{E}+a)^2+\Gamma^2][(\tilde{E}-a)^2+\Gamma^2]}, \tag{3}$$

where we define the energy related to the dipole moment as $E_d = 4\pi|\mathbf{d}|^2/\varepsilon_b$, and we introduce $\tilde{E} = (E_0 - E) + E_d\left(1 + \frac{1}{2(\varepsilon_b - 1)}\right)$ and $a = \frac{1}{2(\varepsilon_b - 1)}E_d$. Here and below, we assume that the incidence angle θ is small enough so that we can neglect $\tan^2\theta$ with respect to ε_b. As follows from Eqs. (2) and (3) TMOKE is proportional to the damping Γ and exists only within the spectral range where the imaginary part of the permittivity is not vanishing. In this sense, it is similar to the effect of magnetic dichroism. TMOKE grows linearly with Δ and its spectrum has an antisymmetric S-shape with respect to $E = E_0 + E_d\left(1 + \frac{1}{2(\varepsilon_b - 1)}\right)$ (see Figure 2A). TMOKE has a maximum and a minimum spectrally separated by Γ. The magnitudes of TMOKE extrema are directly proportional to the Zeeman splitting Δ:

$$\delta = \mp\frac{3\sqrt{3}E_d \Delta \tan\theta}{2(\varepsilon_b - 1)\Gamma^2}. \tag{4}$$

At the same time, the shape of the TMOKE spectrum does not change with the magnetic field for $\Delta/\Gamma \ll 1$.

Narrow optical resonances in sufficiently large magnetic fields lead to the other limiting case when $\Delta/\Gamma \gg 1$. Analyzing the general expression for TMOKE [Supplementary Eq. (S1)], we should take into account that the resonances of TMOKE are located at $|E_0 - E| = \Delta/2$. We treat Γ/Δ as a small parameter and derive the analytical expression for TMOKE peaks in case $\Delta/\Gamma \gg 1$ (details in Supplementary Section A):

$$\delta = \mp\frac{4\varepsilon_b E_d \tan\theta}{\Gamma} \frac{\varepsilon_b^2 - \varepsilon_b - \frac{E_d^2}{4\Gamma^2}}{\left(\varepsilon_b^2 - \varepsilon_b - \frac{E_d^2}{4\Gamma^2}\right)^2 + \left(\frac{2\varepsilon_b - 1}{2\Gamma}\right)^2 E_d^2} \tag{5}$$

Negative TMOKE refers to $E_0 - E > 0$ and positive TMOKE corresponds to $E_0 - E < 0$. TMOKE spectra for the strong coupling regime are presented in Figure 2B. Contrary to the previous situation of weak coupling, the relatively large magnetic field changes the shape of the TMOKE spectrum when $\Delta > \Gamma$: it comprises two separate peaks of opposite sign, and the energy distance between the peaks corresponds to the Zeeman splitting Δ and consequently increases with the applied magnetic field. Another interesting feature of the strong coupling regime is the fact that the TMOKE peak magnitude experiences saturation. When Δ and Γ are almost equal, one can see that the TMOKE peaks behave like in the weak coupling regime, and the maximal TMOKE gradually grows. However, this initial increase of TMOKE ceases, when the ratio Δ/Γ exceeds about 5. Now, the relatively large Zeeman splitting approximation is fulfilled. Henceforth, the maximum value of TMOKE does not depend on Δ. Similarly to the weak coupling regime, the dependence of TMOKE on the incidence angle is linear as one can see from Eq. (5).

Thus, in large magnetic fields, when the Zeeman splitting exceeds the resonance linewidth, one can observe novel features that do not exist in case of small magnetic fields. Namely, the TMOKE spectrum shape changes with magnetic field: it has two peaks of opposite sign and these peaks move away from each other with increasing magnetic field. Moreover, in contrast to the weak coupling regime, the peak magnitude does not depend on the applied magnetic field. These general features have been

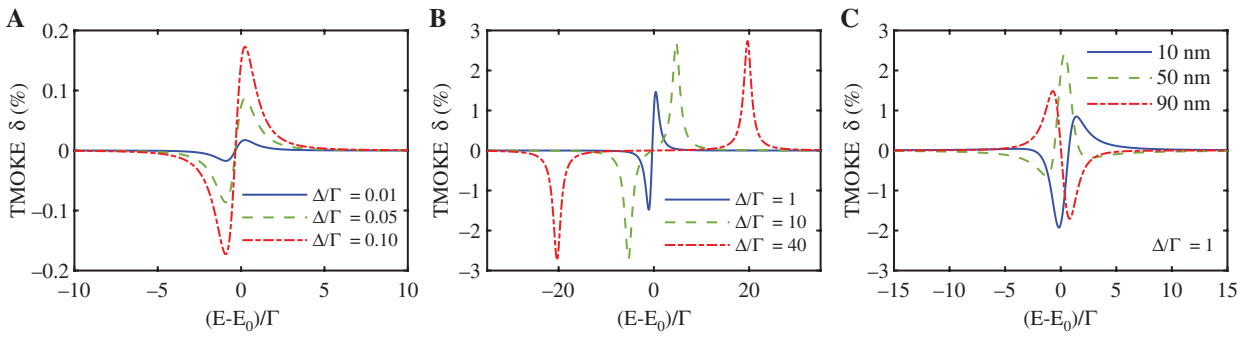

Figure 2: (A and B) TMOKE spectra for various Δ/Γ ratios calculated by Eqs. (1) and (2). Incidence angle $\theta = 20°$, $\Gamma = 2$ meV, $E_d = 0.65$ meV, $E_0 = 1.68$ meV, and $\varepsilon_b \approx 10$. (C) Calculated TMOKE spectra of the 10-nm-thick magnetic film acting as a QW buried at three various distances from the sample surface. Incidence angle $\theta = 20°$, $\Gamma = 2$ meV, $E_d = 0.65$ meV, $\Delta = 2$ meV, $E_0 = 1.68$ meV, and $\varepsilon \approx 8$ for cap and epilayer. In all plots, the dependencies on the relative change of energy with respect to the resonance linewidth are given.

ascertained for the simplest case when the *p*-polarized beam is reflected from a semi-infinite magnetic material with one narrow resonance. For more complex systems, additional peculiarities emerge, nevertheless preserving the general properties discussed above.

As confined quantum states can be formed not only near the sample surface but also at some region in the bulk (e.g. in the QW inside a semiconductor sample with a cap layer), it is important to consider the case when the magneto-optical resonance appears in a thin layer buried at some distance from the sample surface. Although TMOKE is considered as a surface-sensitive effect, in this case, it can be useful for probing confined resonances in depth. For this purpose, we analyze a trilayer structure composed of the cap layer of varying thickness, the 10-nm-thick QW layer with the dielectric permittivity tensor given by Eq. (2), and the buffer layer (see Figure 3A). The variation of the cap layer thickness modifies the shape of TMOKE resonance with a period of 120 nm, which is half of the light wavelength in the cap layer (Figure 2C). Additionally, one can achieve a fully antisymmetric TMOKE spectral shape as it occurs for the 90 nm cap layer.

The TMOKE features discussed above can be observed in different systems that possess sharp optical resonances originating from confined quantum states. In the next section, we concentrate on the experimental demonstration of these features for the case of exciton resonances in magnetic semiconductor QW structures.

2.2 TMOKE at the exciton resonance in semiconductor QW

To investigate TMOKE mediated by excitons in a DMS, we use a sample with a QW structure grown by molecular-beam epitaxy on a (001)-oriented GaAs substrate. The 10-nm-thick DMS $Cd_{0.974}Mn_{0.026}Te$ QW layer is sandwiched between nonmagnetic $Cd_{0.73}Mg_{0.27}Te$ barriers (buffer and cap layers; see Methods and Figure 3A). TMOKE measurements were performed in two regimes: (i) the weak coupling regime in magnetic field of $B = 580$ mT at a temperature $T \approx 10$ K and (ii) the strong coupling regime where the magnetic field was varied in 125 mT steps from 0.5 to 5.0 T at $T = 2$ K. For the first case, TMOKE spectra were obtained in a wide range of incidence angles using a Fourier imaging setup. In the second case, the measurements were performed for $\theta = 5°$. In both cases, the magnetic field was oriented in the QW plane and perpendicular to the plane of light incidence as shown in Figure 3A. The details on the measurement procedure and evaluation of TMOKE spectra are presented in Section 4.

2.3 TMOKE in the weak coupling regime

Figure 4 summarizes the data obtained in the weak coupling regime of excitonic states. Reflection spectra of the structure show oscillations related to the interference of light after multiple reflections within the (Cd,Mg)Te buffer layer (Figure 4A, solid curve). The exciton resonance from the DMS QW is represented by a weak feature in the reflection spectrum at a photon energy of about 1.683 eV. In contrast, the TMOKE spectrum presented in Figure 4B at $\theta = 5°$ shows a much more abundant picture with two resonances located at 1.683 and 1.701 eV. This result highlights the sensitivity of TMOKE spectroscopy.

The presence of two exciton resonances in the TMOKE spectrum of the DMS QW structure is related to the quantization of carriers inside the QW as well as uniaxial strain in the direction along the normal to the QW [27]. For that

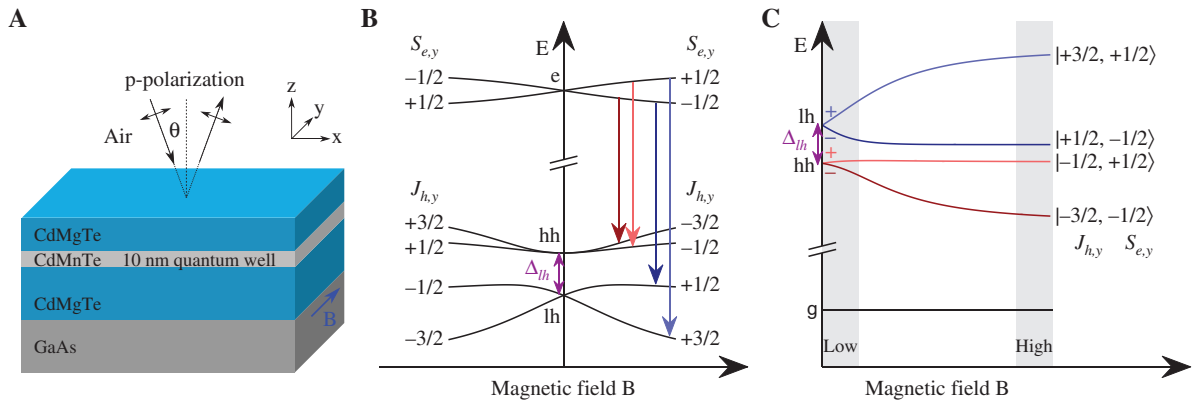

Figure 3: (A) Schematic presentation of the studied DMS QW structure and geometry of the experiment under light incidence. Magnetization **M** and external magnetic field **B** are oriented in the QW plane. (B) Energy diagram and Zeeman splitting of conduction and valence band states in Voigt geometry (single particle picture). Vertical lines indicate the relevant dipole-allowed optical transitions with elliptical polarization in *xz*-plane (optical transitions with linear polarization along magnetic field direction are not considered here). Red/blue lines correspond to σ^+/σ^- polarization in the *xz*-plane in the limit of large magnetic fields where the electron and hole eigenstates are defined by the angular momentum projections on magnetic field direction $S_{e,y}$ and $J_{h,y}$, respectively. At $B=0$, the hh and lh states are split by Δ_{lh}. (C) Energy diagram from (B) in the exciton picture. Gray areas indicate the limiting cases of low and high magnetic fields. For low magnetic fields, the upper two transitions correspond to the lh exciton ($lh_{+,-}$, light and dark blue lines, respectively), whereas the lower ones correspond to the hh exciton ($hh_{+,-}$, light and dark red lines, respectively). Due to admixture from the lh to the hh, the states at high magnetic field are denoted as labeled within the figure. The labeling of exciton states in this case is given by the $|J_{h,y}, S_{e,y}\rangle$ notation.

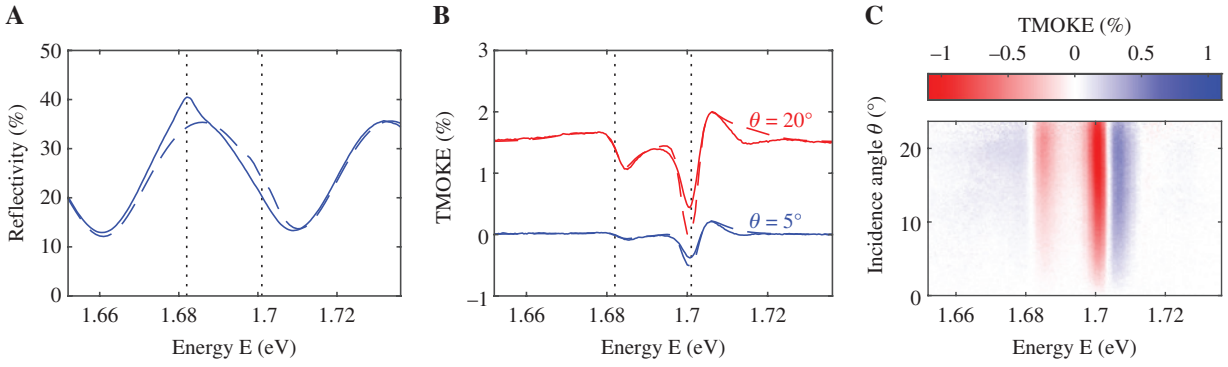

Figure 4: (A) Reflectivity spectrum from experiment (solid line) and theory (dashed line) at an incidence angle of $\theta=5°$ and $T=10$ K. (B) TMOKE spectra for $\theta=5°$ (blue) and $\theta=20°$ (red) at $B=580$ mT and $T=10$ K. The curves obtained for $\theta=20°$ are shifted upward by 1.5% for clarity. Solid line refers to the experiment and dashed line corresponds to the theory. (C) Angular-resolved TMOKE spectrum in the excitonic spectral range in the case of a weak coupling regime at $B=580$ mT and $T=10$ K. Δ/Γ is different for lh and hh contributions: 1.79 for lh and 0.5 for hh.

reason, the light-hole (*lh*) and heavy-hole (*hh*) exciton resonances, which are degenerate in a bulk crystal, split into the *lh* state with $E_{lh}(B=0)=1.701$ eV and the *hh* state with $E_{hh}(B=0)=1.683$ eV. The corresponding energies are marked by dotted vertical lines in Figure 4A and B. The light-heavy-hole splitting is equal to $\Delta_{lh}=18$ meV. Both TMOKE resonances are observed for oblique incidence near the frequencies of the corresponding transitions from the hole states and have antisymmetric S-shape. The exciton-mediated TMOKE grows with increase of the incidence angle, reaching 1.1% at $\theta=20°$ (Figure 4C), which is several orders of magnitude larger than the off-resonant value of 0.01%, observed at $\theta=20°$ and photon energy around 1.58 eV.

We emphasize that the lh exciton feature in the photoluminescence and reflectivity spectra is too weak to determine the position of the resonance, which is mainly due to its fast relaxation into the ground state corresponding to the hh exciton. In contrast, the TMOKE spectrum can be used to determine the positions of both exciton resonances. Interestingly, the strength of TMOKE is about twice larger for lh excitons than for the hh state and the sign of the effect is opposite. In other words, for positive

incidence angle θ, the TMOKE magnitude for the lh exciton changes from positive to negative values with increasing photon energy E (rising S-shape), whereas for the hh exciton an opposite behavior with decreasing S-shape is observed as shown in Figure 4B.

Heavy-hole excitons show a smaller magnitude of TMOKE because at zero magnetic field the corresponding transitions are linearly polarized in the QW plane and hence carry zero spin along the magnetic field direction. Hence, TMOKE for the hh resonance is enabled only due to the admixture of lh states at nonzero magnetic field. That explains why the hh TMOKE remains relatively weak until the Zeeman splitting becomes comparable to the light-heavy-hole splitting. It also hints to the origin of the different sign for light-holes and heavy-holes, which will be explained more intuitively once we consider higher magnetic fields.

Now, we proceed to a quantitative description of the TMOKE resonance for hybridized lh and hh states at weak magnetic field. To that end, we have calculated the effective permittivity tensor of the QW. The orbital effects of the magnetic field, which can mix lh and hh resonances and induce spatial dispersion [28], were neglected. In the case of a DMS structure, these effects are less important than the Mn-mediated giant Zeeman splitting. The resulting QW permittivity tensor can be presented as $\varepsilon = \varepsilon_b(1+\chi_{hh}+\chi_{lh})$, with the hh and lh susceptibilities in the xz subspace (Ox is in the QW plane and perpendicular to the external field and Oz is normal to the QW plane; see Figure 3A). The susceptibilities read (see Section B of Supplementary Materials for the derivation details):

$$\chi_{hh} = \frac{\hbar\omega_{LT} D_{hh}}{D_{hh,+} D_{hh,-}} \begin{pmatrix} \mathcal{Z}^2 & \mathrm{i}\mathcal{Z}/3 \\ -\mathrm{i}\mathcal{Z}/3 & 1 \end{pmatrix}, \tag{6}$$

$$\chi_{lh} = \frac{\hbar\omega_{LT} D_{lh}}{D_{lh,+} D_{lh,-}} \begin{pmatrix} \frac{4}{3} & -\frac{\mathrm{i}}{3}\left(\frac{E_{lh,-}-E_{lh,+}}{D_{lh}} + \mathcal{Z}\right) \\ \frac{\mathrm{i}}{3}\left(\frac{E_{lh,-}-E_{lh,+}}{D_{lh}} + \mathcal{Z}\right) & \frac{1}{3} \end{pmatrix}.$$

Here, $D_\nu \equiv E_\nu - E - \mathrm{i}\Gamma_\nu$; E_ν and Γ_ν are the exciton resonance energy and width, the index $\nu = lh, hh, (lh,\pm), (hh,\pm)$ labels zero-field and Zeeman-split excitonic transition energies (see also Figure 3C), and ω_{LT} is the effective longitudinal-transverse splitting. The parameter $\mathcal{Z}$ depends linearly on the magnetic field being responsible for the light-heavy-hole mixing. It is determined by the ratio of the Zeeman splitting of the hh state in the Faraday configuration $\Delta_{h,F}$ to the light-heavy-hole splitting Δ_{lh}. For the experimentally relevant case of $B = 580$ mT, it is equal to $|\mathcal{Z}| \approx 0.3$. In the general case, one has $\mathcal{Z} = N_0\beta x S B_S / \Delta_{lh}$, where $N_0\beta = -0.88$ eV is the $p-d$ exchange interaction constant, $S = 5/2$ is the Mn spin, x is the concentration of Mn^{2+} ions, and $B_S(\kappa)$ is the modified Brillouin function describing the magnetization of Mn ions at given magnetic field and temperature [20, 22, 23, 29]. For $S = 5/2$, the argument of $B_S(\kappa)$ is defined as $\kappa = 5\mu_B g_{Mn} B/2k_B T_{eff}$ with the Bohr magneton μ_B, the Boltzmann constant k_B, the Landé factor of Mn^{2+} ion $g_{Mn} = 2.01$, and the effective temperature $T_{eff} = T + T_0$. The specific parameters of the investigated structure $x \approx 0.026$ and $T_0 \approx 1.5$ K were evaluated from the magnetic field dependence of hh exciton splitting in the Faraday geometry $\Delta_{h,F}$ measured using photoluminescence spectroscopy [30].

The TMOKE response is described by the off-diagonal elements of the susceptibilities (6). The different signs before these elements for lh and hh reflect different signs of the TMOKE response. Because of the term $\propto (E_{lh,-} - E_{lh,+})/D_{lh}$, for light-holes, TMOKE is possible even when the mixing with the heavy-holes is neglected, i.e. $\mathcal{Z} \to 0$. Note that the mixing term $\mathcal{Z}$ is determined solely by the energy structure of the valence band states, i.e. proportional to $\Delta_{h,F}/\Delta_{lh}$, whereas the energy splitting of the exciton resonances is governed by the Zeeman splitting of both valence band and conduction band states as shown in Figure 3B and C. The contribution from the electrons is given by $\Delta_e = N_0\alpha x S B_S$, where $N_0\alpha = 0.22$ eV is the $s-d$ exchange interaction constant between the conduction band electrons and Mn^{2+} ions in (Cd,Mn)Te. The corresponding splittings for lh and hh excitons are given by $\Delta_{X,\nu} = E_{\nu,+} - E_{\nu,-} + \Delta_e$ with $\nu = lh, hh$, respectively. A detailed description of the magnetic field induced splitting of exciton resonances in the Voigt geometry is given in Section B of Supplementary Materials.

Using the transfer matrix method for multilayer DMS structures with the QW described by Eq. (6), we calculated the reflectance and TMOKE spectra. They show good agreement with the experimental data if $E_{lh} = 1.7005$ eV and $E_{hh} = 1.6825$ eV are assumed (Figure 4A and B, dashed curves). The longitudinal-transverse splitting is $\hbar\omega_{LT} = 0.65$ meV, whereas the linewidth and Zeeman splitting of both resonances are $\Gamma_{hh} = \Gamma_{lh} = 2.4$ meV, $\Delta_{X,hh} = 1.2$ meV, and $\Delta_{X,lh} = 4.3$ meV. Therefore, in the external magnetic field of 580 mT, Δ is of the order of Γ, and in Figure 4B and C, we deal with the weak coupling regime.

2.4 TMOKE in the strong coupling regime

As the exciton resonances are quite narrow, the strong coupling regime ($\Delta/\Gamma \gg 1$) is already reachable in magnetic fields of several Tesla, i.e. if the temperature is kept

low enough ($T=2$ K) that the ratio Δ/Γ exceeds 5 at $B=2$ T and is about 10 at $B=5$ T.

TMOKE spectra and their dependence on magnetic field strength up to 5 T for $\theta=5°$ are presented in Figure 5. It follows that for $\Delta/\Gamma \gg 1$ each of the resonant TMOKE features corresponding to hh and lh excitons at $B=0$ split into two resonance features. The splitting increases with the increase of B. Remarkably, TMOKE maximum/minimum values are saturated at $B=1$ T and remain constant for higher fields. Consequently, in this regime, the magnetic field influences the shape of the TMOKE spectrum but does not increase its value of $\delta=0.5\%$.

To interpret the four branches in TMOKE spectra at higher B, let us consider the case of the Zeeman energy, which overcomes the light-heavy-hole splitting ($\mathcal{Z} \gg 1$) in magnetic fields higher than 1 T (see Figure 3). In this regime, a simple qualitative picture can be considered, which is realized in a bulk (Cd,Mn)Te crystal. In Voigt configuration ($\mathbf{B}||y$), the Zeeman-split electron states are characterized by the spin projection $S_{e,y}=\pm 1/2$ representing a doublet. The valence band states split into a quartet with Zeeman energy governed by the total angular momentum projection on the magnetic field direction $J_{h,y}=\pm 1/2, \pm 3/2$. Note that the case of strong magnetic field is fundamentally different from the case of weak magnetic field where the quantization axis is given by the QW confinement potential; therefore, the energies of the valence band states are mainly determined by the normal projection of the angular momentum $J_{h,z}=\pm 1/2, \pm 3/2$ for lh and hh, respectively.

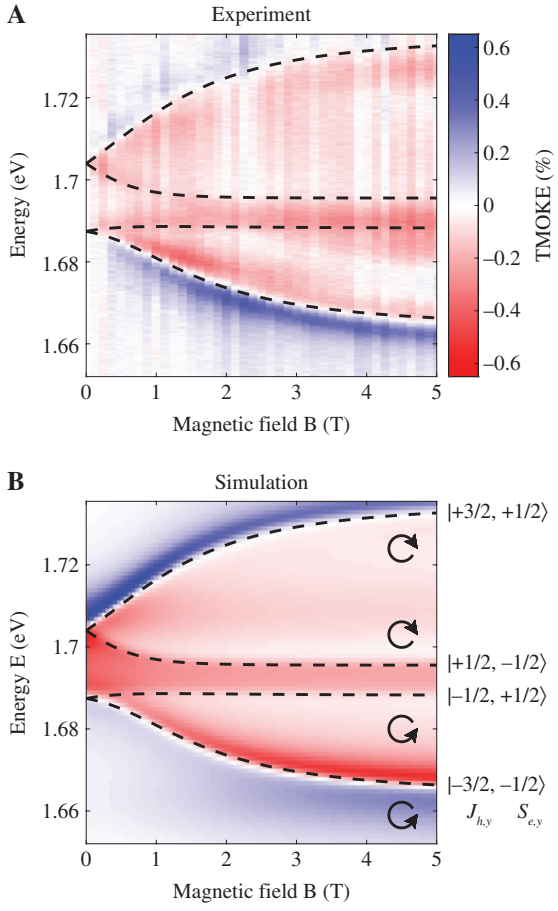

Figure 5: TMOKE in the excitonic spectral range in the strong coupling regime $\Delta/\Gamma>1$: (A) measured and (B) calculated energy and magnetic field resolved TMOKE spectra for $\theta=5°$ at $T=1.6$ K.

Neglecting the QW confinement, the splittings of conduction and valence band states are given by $\Delta_e = 2N_0\alpha x\,|S_{e,y}|\,B_S$ and $\Delta_h = -\frac{2}{3}N_0\beta x\left|J_{e,y}\right|B_S$, respectively. Thus, we obtain four σ-polarized exciton transitions. The energy splitting between the outer hh-like components $\Delta_{out}=\Delta_h+\Delta_e$ correspond to the excitonic states $|\pm 3/2, \pm 1/2\rangle$ written in the $|J_{h,y},S_{e,y}\rangle$ notation. The inner components are split by $\Delta_{in}=\Delta_h/3-\Delta_e$ corresponding to lh-like exciton resonances $|\pm 1/2, \mp 1/2\rangle$. Following Figure 5, the splitting $\Delta_{out}\approx 70$ meV, whereas Δ_{in} is about eight times smaller at $B=5$ T. According to the $s-d$ and $p-d$ exchange constants in bulk (Cd,Mn)Te, the relation $\Delta_{out}>\Delta_{in}>0$ holds [20]. In this case, the two optical transitions with lower energy $|-3/2, -1/2\rangle$ and $|-1/2, +1/2\rangle$ are σ^+-polarized in the xz-plane, while the upper energy transitions $|+3/2, +1/2\rangle$ and $|+1/2, -1/2\rangle$ have opposite σ^- polarization (see also Figure 3C). The form of the S-shaped resonances in large magnetic field is in full accord with this considerations: it has a rising slope for the low-energy exciton transitions at 1.666 and 1.688 eV and changes to falling for the higher-energy resonances at 1.696 and 1.733 eV. This also explains the opposite sign of the lh and hh TMOKE resonances observed in the limit of small magnetic fields (Figure 4).

The susceptibilities at large fields can be simplified to a compact antisymmetric form (Supplementary Section B):

$$\chi_{hh} = \frac{\hbar\omega_{LT}}{6}\begin{pmatrix} U_{hh} & -iW_{hh} \\ iW_{hh} & U_{hh} \end{pmatrix}, \qquad (7)$$

$$\chi_{lh} = \frac{\hbar\omega_{LT}}{2}\begin{pmatrix} U_{lh} & iW_{lh} \\ -iW_{lh} & U_{lh} \end{pmatrix}$$

where $U_\nu = \frac{1}{D_{\nu,+}}+\frac{1}{D_{\nu,-}}$ and $W_\nu = \frac{1}{D_{\nu,+}}-\frac{1}{D_{\nu,-}}$, and $\nu = lh, hh$. It allows one to calculate the position of the four exciton states versus the magnetic field (Figure 5, dashed curves) and satisfactory describe the experimental TMOKE map for large magnetic fields (Figure 5B). In particular, this model also predicts the saturation of TMOKE in higher magnetic fields.

3 Discussion

To conclude, we have demonstrated here the enhancement of TMOKE in the vicinity of a narrow optical resonance. There are two distinct TMOKE regimes that depend on the magnitude of the Zeeman splitting with respect to the linewidth. In the weak coupling regime ($\Delta < \Gamma$), the TMOKE magnitude grows linearly with the increase of the Zeeman splitting and its spectrum has an S-shape. On the contrary, in the strong coupling regime ($\Delta > \Gamma$), the TMOKE magnitude saturates, whereas its spectrum is strongly modified with the increase of the Zeeman splitting leading to the appearance of two separate TMOKE peaks. The spectral dependence of the TMOKE peaks and the sign of δ provide rich information on the energy structure and selection rules for optical transitions.

Although in this work the considered phenomena were experimentally demonstrated at the exciton resonances in a 10-nm-thick (Cd,Mn)Te/(Cd,Mg)Te QW, they can also be found in other physical systems. For example, the optical resonances of the rare-earth ions in dielectric materials are quite narrow so that $\Gamma \leq \Delta$ even in moderate magnetic fields. In this respect, X-ray spectra of the confined quantum states are of interest [18, 31, 32]. For instance, the rare-earth ions in orthoborates provide lines with $\Delta/\Gamma \approx 1$ in $B \approx 1$ T [18]. Apart from X-ray, the visible and infrared spectra also demonstrate narrow lines [19, 33–36].

Our results have several implications in fundamental and applied optics. First, resonant TMOKE in the strong coupling regime can be used as a spectroscopic tool for the investigation of the energy structure of electronic states that are involved in optical transitions. It should be noted that although TMOKE is usually considered as a surface sensitive effect, it is demonstrated here to be applicable for probing confined resonances in the depth of the sample as well.

Next, resonant TMOKE can be used to read out the in-plane magnetization of the system, which is appealing for possible applications in quantum information and sensing technologies [37, 38]. Typically, the spin dynamics in semiconductors is assessed by the polarization rotation due to the Faraday effect or Polar Kerr effect (PMOKE) [39]. However, these give access only to one of the spin components parallel to the direction of light propagation ($\mathbf{B} \,||\, \mathbf{k}$). On the contrary, TMOKE allows measuring the perpendicular component of the magnetization. Thus, a combination of TMOKE and PMOKE provides the possibility for performing spin tomography.

4 Methods

To investigate TMOKE mediated by excitons in a DMS, we used a QW structure grown by molecular-beam epitaxy on a 400-µm-thick (001)-oriented GaAs substrate. The 10-nm-thick magnetic $Cd_{0.974}Mn_{0.026}Te$ QW layer is sandwiched between nonmagnetic $Cd_{0.73}Mg_{0.27}Te$ barriers (3.25-µm-thick buffer and 250-nm-thick cap layer, respectively). Qualitatively, the same results were obtained with another sample. The 10-nm-thick QW layer was sandwiched in between 3.05-µm-thick buffer and 30-nm-thick cap layer. The only difference observed is the change of TMOKE spectral shape as discussed above in Section 2.1 and shown in Figure 2C.

The experimental studies were performed on the following two set-ups. In the weak coupling regime, the sample was placed in a He flow cryostat between the ferrite cores of an electromagnet. Fourier imaging spectroscopy was used to measure the angular- and wavelength-resolved reflectivity and TMOKE spectra at low temperatures of about 10 K using a tungsten halogen lamp, which illuminates the sample with *p*-polarized light. The reflected light was collimated using a microscope objective with numerical aperture of 0.4, resulting in the experimentally accessible angular range of ±23°. A telescope consisting of two achromatic doublets mapped the collimated light onto the spectrometer slit. The exit slit of the spectrometer was equipped with a thermoelectric cooled charge-coupled device (CCD) detector, providing a spectral resolution of 0.6 nm and an angular resolution of about 0.4°. By taking the reflected intensity for two opposite magnetic field directions, the parameter δ characterizing TMOKE was deduced. For these rather low magnetic field strengths, the noise level is reduced by repetitive switching of the magnetic field direction. This also smoothes potential fluctuations of the lamps intensity.

On the contrary, in the giant Zeeman splitting case, the sample was kept at a temperature of 1.6 K inside a liquid helium bath cryostat equipped with a split-coil superconducting magnet. Transverse magnetic fields of up to 5 T were applied to observe the magnetic field induced change of reflectivity for *p*-polarized white light incident under an angle of 5°. The reflected light was subsequently dispersed by the spectrometer and detected with the CCD detector. The sweeping of the current in the superconducting magnet is slow; therefore, it does not allow to perform repetitive measurements in two opposite magnetic fields within a reasonable time. Therefore, we swept the magnetic field once in steps of 125 mT from −5 to 5 T and back again. For each magnetic field step, we

measured the reflected intensity multiple times in both *p*- and *s*-polarizations. In this case, potential intensity fluctuations of the white light source are smoothed by normalizing each *p*-polarized spectrum to the spectrally integrated *s*-polarized intensity for each magnetic field step $I_p(B, \omega)/I_s(B)$. Using the spectrally integrated *s*-polarized intensity for normalization has the advantage that otherwise small temperature deviations might slightly shift the optical resonances and consequently change the spectral dependence of TMOKE.

Acknowledgments: This study was supported by the Deutsche Forschungsgemeinschaft via ICRC TRR 160 (Project C5), the Russian Foundation for Basic Research (project no. 16-32-60135 mol_a_dk), and the Foundation for the Advancement of Theoretical Physics BASIS. The research in Poland was partially supported by the National Science Centre (grant no. UMO-2017/25/B/ST3/02966) and the Foundation for Polish Science through the IRA Programme cofinanced by the European Union within SG OP.

References

[1] Zvezdin A, Kotov V. Modern magnetooptics and magnetooptical materials. Bristol, IOP, 1997.
[2] Soldatov IV, Schäfer R. Selective sensitivity in Kerr microscopy. Rev Sci Instrum 2017;88:073701.
[3] Hubert A, Schäfer R. Magnetic domains. The analysis of magnetic microstructures. New York, Springer, 1998.
[4] Kuch W, Schäfer R, Fischer P, Hillebrecht F. Magnetic microscopy of layered structures. New York, Springer, 2015.
[5] Kalish AN, Belotelov VI. Magneto-optical effects for detection of in-plane magnetization in plasmonic crystals. Phys Solid State 2016;58:1563.
[6] Bonod N, Reinisch R, Popov E, Nevìere M. Optimization of surface-plasmon-enhanced magneto-optical effects. J Opt Soc Am B 2004;21:791–7.
[7] Krinchik GS, Artem'ev VA. Magneto-optical properties of Ni, Co and Fe in the UV, visible, and infrared parts of the spectrum. Zh Eksp Teor Fiz 1967;53:1901.
[8] Belotelov VI, Akimov IA, Pohl M, et al. Enhanced magneto-optical effects in magnetoplasmonic crystals. Nat Nanotech 2011;6:370.
[9] Borovkova OV, Hashim H, Kozhaev MA, et al. TMOKE as efficient tool for the magneto-optic analysis of ultra-thin magnetic films. Appl Phys Lett 2018;112:063101.
[10] Chekhov AL, Krutyanskiy VL, Shaimanov AN, Stognij AI, Murzina TV. Wide tunability of magnetoplasmonic crystals due to excitation of multiple waveguide and plasmon modes. Opt Express 2014;22:17762–8.
[11] Sylgacheva D, Khokhlov N, Kalish A, et al. Transverse magnetic field impact on waveguide modes of photonic crystals. Opt Lett 2016;41:3813–6.
[12] Vinogradov A, Dorofeenko AV, Merzlikin AM, Lisyansky A. Surface states in photonic crystals. Physics-Uspekhi 2010;53:243.
[13] Borovkova O, Kalish A, Belotelov V. Transverse magneto-optical Kerr effect in active magneto-plasmonic structures. Opt Lett 2016;41:4593–6.
[14] Bossini D, Belotelov VI, Zvezdin AK, Kalish AN, Kimel AV. Magnetoplasmonics and femtosecond optomagnetism at the nanoscale. ACS Photonics 2016;3:1385–400.
[15] Ferreiro-Vila E, Khokhlov N, Kalish A, et al. Magneto-optical and magnetoplasmonic properties of epitaxial and polycrystalline Au/Fe/Au trilayers. Phys Rev B 2011;83:205120.
[16] Ignatyeva DO, Knyazev GA, Kapralov PO, Dietler G, Sekatskii SK, Belotelov VI. Magneto-optical plasmonic heterostructure with ultranarrow resonance for sensing applications. Sci Rep 2016;6:28077.
[17] Pohl M, Kreilkamp LE, Belotelov VI, et al. Tuning of the transverse magneto-optical Kerr effect in magneto-plasmonic crystals. N J Phys 2013;15:075024.
[18] Yagupov S, Strugatsky M, Seleznyova K, et al. Iron borate films: synthesis and characterization. J Magn Magn Mater 2016;417:338–43.
[19] Rare-Earth-Doped Fiber Lasers and Amplifiers. 2nd ed. Digonnet MJF, ed. New York, CRC Press, 2001.
[20] Kossut J, Gaj JA. In: Introduction to the physics of diluted magnetic semiconductors. Kossut J, Gaj JA, eds. Berlin, Springer, 2010:1–36.
[21] Kotova LV, Platonov AV, Kats VN, Shamirzaev TS, André R, Kochereshko VP. Nonreciprocal optical and magnetooptical effects in semiconductor quantum wells. Phys Solid State 2018;60:2269–75.
[22] Gaj J, Galazka R, Nawrocki M. Giant exciton Faraday rotation in $Cd_{1-x}Mn_xTe$ mixed crystals. Solid State Commun 1978;25:193–5.
[23] Furdyna JK. Diluted magnetic semiconductors. J Appl Phys 2010;64:R29–64.
[24] Feynman RP, Vernon FL, Hellwarth RW. Geometrical representation of the Schrödinger equation for solving Maser problems. J Appl Phys 1957;28:49–52.
[25] Dzhioev RI, Gibbs HM, Ivchenko EL, et al. Determination of interface preference by observation of linear- to-circular polarization conversion under optical orientation of excitons in type-II GaAs/AlAs superlattices. Phys Rev B 1997;56:13405–13.
[26] Scully MO, Zubairy MS. Quantum optics. Chapter 7. Cambridge, UK, Cambridge University Press, 1997.
[27] Ivchenko EL. Optical spectroscopy of semiconductor nanostructures. Harrow, UK, Alpha Science International, 2005.
[28] Kotova LV, Kats VN, Platonov AV, Kochereshko VP, André R, Golub LE. Magnetospatial dispersion of semiconductor quantum wells. Phys Rev B 2018;97:125302.
[29] Kuhn-Heinrich B, Ossau W, Bangert E, Waag A, Landwehr G. Zeeman pattern of semimagnetic (CdMn)Te/(CdMg)Te quantum wells in inplane magnetic fields. Solid State Commun 1994;91:413–8.
[30] Spitzer F, Poddubny AN, Akimov IA, et al. Routing the emission of a near-surface light source by a magnetic field. Nat Phys 2018;14:1043–8.
[31] Fukui K, Ogasawara H, Harada I, Kotani A. Magnetic circular dichroism of resonant X-ray emission spectra at L edges of rare-earth compounds. J Synchrotron Radiat 2001;8:407–9.
[32] Kang Z, Zhang Y, Menkara H, et al. CdTe quantum dots and polymer nanocomposites for X-ray scintillation and imaging. Appl Phys Lett 2011;98:181914.

[33] Agrawal GP. Applications of nonlinear fiber optics. 2nd ed. Amsterdam, Academic Press – Optics and Photonics Series, 2008.
[34] Vinh NQ, Przybylińska H, Krasil'nik ZF, Gregorkiewicz T. Microscopic structure of Er-related optically active centers in crystalline silicon. Phys Rev Lett 2003;90:066401.
[35] Borovikova EY, Aksenov SM, Dobretsova EA, et al. Crystal growth, structure, infrared spectroscopy, and luminescent properties of rare-earth gallium borates $RGa_3(BO_3)_4$, R=Nd, Sm-Er, Y. Opt Mater 2016;49:304–11.
[36] Popova MN. Spectroscopy of compounds from the family of rare-earth orthoborates. J Rare Earths 2009;27:607–11.
[37] Weber JR, Koehl WF, Varley JB, et al. Quantum computing with defects. Proc Natl Acad Sci 2010;107:8513–8.
[38] Dyakonov MI, ed. Spin physics in semiconductors. Springer International Publishing, 2017.
[39] Buda B, Dahl M, von Truchsess N, Waag A. Polar magneto-optic Kerr effect in (Cd, Mn)Te/CdTe superlattices. J Cryst Growth 1994;138:652–5.

Supplementary Material: The online version of this article offers supplementary material (https://doi.org/10.1515/nanoph-2018-0187).